Sādhanā Vol. 36, Part 3, June 2011, pp. 371–391. © Indian Academy of Sciences

Effects of CuO nanoparticles on compressive strength of self-compacting concrete

ALI NAZARI* and SHADI RIAHI

Department of Materials Science and Engineering, Saveh Branch, Islamic Azad University, Saveh 39187-366, Iran
e-mail: alinazari84@aut.ac.ir

MS received 31 August 2010; revised 18 December 2010; accepted 24 February 2011

Abstract. In the present study, the compressive strength, thermal properties and microstructure of self-compacting concrete with different amounts of CuO nanoparticles have been investigated. CuO nanoparticles with an average particle size of 15 nm were added to self-compacting concrete and various properties of the specimens were measured. The results indicate that CuO nanoparticles are able to improve the compressive strength of self-compacting concrete and reverse the negative effects of superplasticizer on compressive strength of the specimens. CuO nanoparticles as a partial replacement of cement up to 4 wt.% could accelerate C–S–H gel formation as a result of the increased crystalline $Ca(OH)_2$ amount at the early ages of hydration. Increasing CuO nanoparticle content to more than 4 wt.%, causes reduced compressive strength because of unsuitable dispersion of nanoparticles in the concrete matrix. Accelerated peak appearance in conduction calorimetry tests, more weight loss in thermogravimetric analysis and more rapid appearance of peaks related to hydrated products in X-ray diffraction results, all indicate that CuO nanoparticles up to 4 wt.% could improve the mechanical and physical properties of the specimens. Finally, CuO nanoparticles improved the pore structure of concrete and caused shifting of the distributed pores from harmless to low harm.

Keywords. SCC; CuO nanoparticles; compressive strength; pore structure; thermogravimetric analysis.

1. Introduction

Self-compacting concrete (SCC) is one of the most significant advances in concrete technology in recent years. SCC may be defined as a concrete with the capacity to flow inside the frame-

*For correspondence

work, to pass around the reinforcements and through the narrow sections, consolidating simply under its own weight without needing additional vibration and without showing segregation or bleeding. This behaviour is achieved in normally vibrated concretes (NVC) in which the same components are used with a higher content of fines and using very powerful superplasticizers. In addition, to increase the viscosity of the paste, viscosity-modifying admixtures can also be used. These are usually comprised of polymers made up of long-chain molecules which are capable of absorbing and fixing the free water content. This modification in the mix design may have an influence on the mechanical properties of the concrete; therefore it is important to ensure that all the basic assumptions and test results for design models of NVC construction are also valid for SCC construction.

Most articles which are published until now show that for a certain compressive strength, SCC tend to reach strength slightly higher than that of NVC (Köning *et al* 2001; Hauke 2001 and Fava *et al* 2003). Mostly, all research has used SCC which includes active additions to satisfy the great demand for fines needed for this type of concrete, thereby improving the mechanical properties in comparison with NVC. For instance, Köning *et al* (2001) and Hauke (2001) registered strength increase in SCCs made with different amounts of fly ash. According to Fava *et al* (2003), in SCCs with granulated blast furnace slag this increase is also evident. On the other hand, when limestone filler is used, Fava *et al* (2003) and Daoud *et al* (2003) achieved a tensile strength in SCC lower than the equivalent NVC. Bosiljkov (2003) has illustrated the behaviour of both types of concrete are similar. As for the modulus of elasticity, it is generally seen that this rises with age at a similar rate to that of NVCs (Köning *et al* 2001), though it seems that SCCs are a little more deformable (Makishima *et al* 2001; Klug & Holschemacher 2003 and Chopin *et al* 2003). These small differences in stiffness between the two types of concrete can be attributed to the SCCs' high paste content; although according to Su *et al* (2001), increasing the fine aggregate/total aggregate ratio does not have a significant effect on the SCCs' modulus of elasticity. In any case, it should be pointed out that most of the results available in the bibliography usually refer to high strength SCCs, where high cement contents (higher than 400 kg/m^3) are used, usually accompanied by active additions, such as fly ash or blast furnace slag. However, there are few studies that give results for low to medium compressive strength of SCCs.

To the knowledge of authors, there are few works on incorporating nanoparticles into SCCs to achieve improved physical and mechanical properties. There are several reports on incorporation of nanoparticles in NVCs, most of which have focused on using SiO_2 nanoparticles (Bjornstrom *et al* 2004; Ji 2005 and Jo *et al* 2007). In addition, some of the works have utilized nano-Al_2O_3 (Li *et al* 2006 and Campillo *et al* 2007), nano-Fe_2O_3 (Li *et al* 2004) and zinc–iron oxide nanoparticles (Flores-Velez & Dominguez 2002). Previously, the effects of SiO_2 (Nazari & Riahi 2010a), TiO_2 [Nazari 2010; Nazari & Riahi 2010b, 2010c) and ZnO_2 (Nazari & Riahi 2010d, 2010e) nanoparticles on different properties of self-compacting concrete have been studied. In addition, in a series of works (Nazari & Riahi 2010f, 2010g, 2010h, 2010i, 2010j, 2010k), the effects of several types of nanoparticles on properties of concrete specimens which are cured in different curing media have been investigated.

Incorporation of other nanoparticles is rarely reported. Therefore, introducing some other nanoparticles which probably could improve the mechanical and physical properties of cementitious composites would be interesting. The aim of this study is incorporating CuO nanoparticles into SCCs to study the compressive strength and pore structure of the concrete. Several specimens with different amounts of polycarboxylate superplasticizer (PC) have been prepared and their physical and mechanical properties have been considered when, instead of cement, CuO nanoparticles were partially added to the cement paste.

Table 1. Chemical and physical properties of Portland cement (*Wt.%*).

Material	SiO_2	Al_2O_3	Fe_2O_3	CaO	MgO	SO_3	Na_2O	K_2O	Loss on ignition
Cement	21.89	5.3	3.34	53.27	6.45	3.67	0.18	0.98	3.21

Specific gravity: 1.7 g/cm^3

2. Materials and methods

Ordinary Portland Cement (OPC) conforming to ASTM C150 standard was used as received. The chemical and physical properties of the cement are shown in table 1. The particle size distribution pattern of the used OPC is illustrated in figure 1.

CuO nanoparticles with an average particle size of 15 nm and 45 $m^2\ g^{-1}$ Blaine fineness from Suzhou Fuer Import & Export Trade Co., Ltd were used as received. The properties of CuO nanoparticles are shown in table 2. Scanning electron micrographs (SEM) and powder X-ray diffraction (XRD) diagrams of CuO nanoparticles are shown in figures 2 and 3.

Crushed limestone aggregates were used to produce self-compacting concretes, with gravel 4/12 and two types of sand. One of them was coarse 0/4, for fine aggregates and the other was fine 0/2, with a very high fines content (particle size <0.063 mm) of 19.2%. The main function of them was to provide a greater volume of fine materials to improve the stability of the fresh concrete.

A polycarboxylate with a polyethylene condensate defoamed based admixture (Glenium C303 SCC) was used. Table 3 shows some of the physical and chemical properties of polycarboxylate admixture used in this study.

Two series of mixtures were prepared in the laboratory trials. C0-SCC series mixtures were prepared with cement, fine and ultra-fine crushed limestone aggregates with 19.2% by weight of ultra-fines and 0%, 0.3%, 0.5%, 0.7% and 1.0% by weight of polycarboxylate admixture replaced by required water for each specimen. N-SCC series were prepared with different contents of CuO nanoparticles with average particle size of 15 nm. The mixtures were prepared with the cement replacement by CuO nanoparticles from 1 to 5 wt.% and 1 wt.% polycarboxylate admixture. The superplasticizer was dissolved in water and then the nano-CuO was added and stirred at a high speed for 3 min. Though nano-CuO cannot be dissolved in water, a small amount of nano-CuO can be dispersed evenly by the superplasticizer. The water to binder ratio

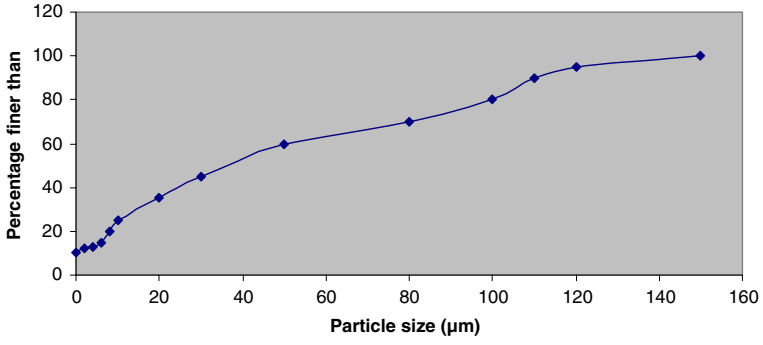

Figure 1. Particles distribution pattern of ordinary Portland cement.

Table 2. The properties of nano-CuO.

Diameter (nm)	Surface volume ratio (m^2/g)	Density (g/cm^3)	Purity (%)
15 ± 3	155 ± 12	<0.13	>99.9

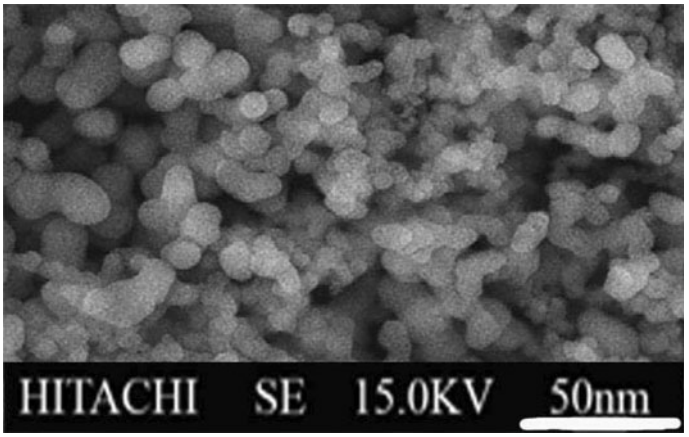

Figure 2. SEM micrograph of CuO nanoparticles.

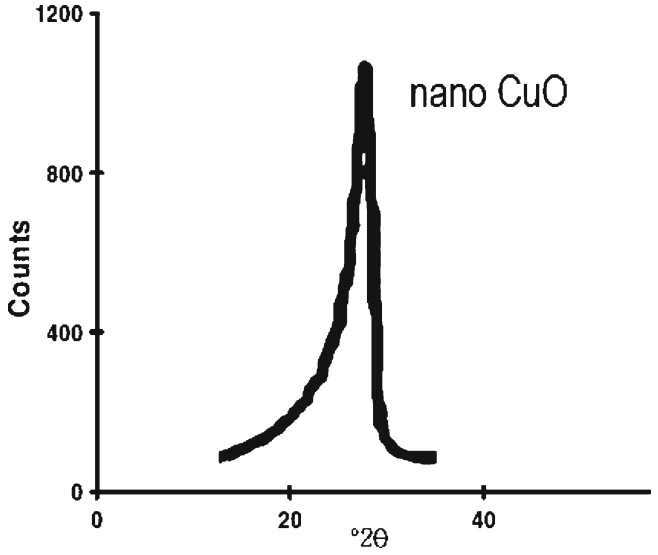

Figure 3. XRD analysis of CuO nanoparticles.

Table 3. Physical and chemical characteristics of the polycarboxylate admixture.

Appearance	Yellow-brown liquid
% solid residue	Approximately 36%
pH	5.2–5.3
Specific gravity (kg/l)	Approximately 1.06
Rotational viscosity (MPa)	79.30
% C	52.25
ppm Na^+	9150
ppm K^+	158

for all mixtures was set at 0.40 (Zivica 2009). The binder content of all mixtures was 450 kgm^{-3}. The proportions of the mixtures are presented in table 4.

The mixing sequence for SCCs consisted of homogenizing the sand and cementitious materials for one minute in the mixer and then adding approximately 75% of the mixing water. The coarse aggregate was introduced and then the superplasticizer was pre-dissolved in the remaining water and was added at the end of the mixing sequence. The total mixing time including homogenizing was 5 minutes.

Several types of tests were carried out on the prepared specimens:

(i) *Compressive strength*: Cubic specimens with 100 mm edge length were made for compressive tests. The moulds were covered with polyethylene sheets and moistened for 24 h. Then the specimens were demoulded and cured in water at a temperature of 20°C in the room condition prior to test days. The compressive strength tests were conducted after 2, 7 and 28 days of curing. Compressive tests were carried out according to the ASTM C 39 standard. After the specified curing period was over, the concrete cubes were subjected to compressive test by using a universal testing machine. The tests were carried out in triplicate and average compressive strength values were obtained.

(ii) *Mercury intrusion porosimetry*: There are several methods generally used to measure the pore structure, such as optical methods, mercury intrusion porosimetry (MIP), helium flow

Table 4. Mixture proportion of nano-CuO particles blended concretes.

Sample designation	CuO nanoparticles (%)	PC content (%)	Quantities (kg/m^3)	
			Cement	CuO nanoparticles
C0-SCC0	0	0	450	0
C0-SCC0.3	0	0.3	450	0
C0-SCC0.5	0	0.5	450	0
C0-SCC0.7	0	0.7	450	0
C0-SCC1	0	1.0	450	0
N1-SCC1	1	1.0	445.5	4.5
N2-SCC1	2	1.0	441.0	9.0
N3-SCC1	3	1.0	437.5	13.5
N4-SCC1	4	1.0	432.0	18.0
N5-SCC1	5	1.0	427.5	22.5

Water to binder [cement + nano-CuO] ratio of 0.40

and gas adsorption (Abell *et al* 1999). The MIP technique is used extensively to characterize the pore structure in porous material as a result of its simplicity, quickness and wide measuring range of pore diameter (Abell *et al* 1999; Tanaka & Kurumisawa 2002). MIP provides information about the connectivity of pores (Abell *et al* 1999).

In this study, the pore structure of concrete was evaluated by using MIP. To prepare the samples for MIP measurement, concrete specimens with 28 days of curing were first broken into smaller pieces, and then the cement paste fragments selected from the center of prisms were used to measure the pore structure. The samples were immersed in acetone to stop hydration as fast as possible. Before the mercury intrusion test, the samples were dried in an oven at about 110°C until reaching constant weight to remove moisture in the pores. MIP is based on the assumption that the non-wetting liquid mercury (the contact angle between mercury and solid is greater than 90) will only intrude in the pores of porous material under pressure (Abell *et al* 1999; Tanaka & Kurumisawa 2002). Each pore size is quantitatively determined from the relationship between the volume of intruded mercury and the applied pressure (Abell *et al* 1999). The relationship between the pore diameter and applied pressure is generally described by the Washburn equation as follows (Abell *et al* 1999; Tanaka & Kurumisawa 2002):

$$D = -4\gamma \cos\theta / P, \tag{1}$$

where, D is the pore diameter (nm), γ is the surface tension of mercury (dyne/cm), θ is the contact angle between mercury and solid (°) and P is the applied pressure (MPa).

The test apparatus used for pore structure measurement was an Auto Pore III mercury porosimeter. Mercury density is 13.5335 g/ml[1]. The surface tension of mercury is taken as 485 dynes/cm[1], and the contact angle selected is 130. The maximum measuring pressure applied is 200 MPa (30000 psi), which means that the smallest pore diameter that can be measured is about 6 nm (on the assumption that all pores are cylindrical in shape).

(iii) *Conduction calorimetry*: This test was run on a Wexham Developments JAF model isothermal calorimeter, using the IBM program AWCAL-4, at 22°C for a maximum of 70 h. Fifteen grams of cement was mixed with water and saturated limewater and admixture before introducing it into the calorimeter cell.

(iv) *Thermogravimetric analysis (TGA):* A Netzsch model STA 409 simultaneous thermal analyzer equipped with a Data Acquisition System 414/1 programmer was used for the tests. Specimens which had been cured for 28 days were heated from 110 to 650°C, at a heating rate of 4°Cmin^{-1} and in an inert N_2 atmosphere.

(v) *Scanning electron microscopy (SEM)*: SEM investigations were conducted on a Hitachi apparatus. Backscattered electron (BSE) and secondary electron (SE) imaging was used to study the samples, which were prepared under conditions that ensured their subsequent viability for analytical purposes.

(vi) *X-ray diffraction (XRD):* A Philips PW-1730 unit was used for XRD analysis which was taken from 4 to 70°.

3. Results and discussion

3.1 *Strength analysis of C0-SCC specimens*

Table 5 shows the compressive strengths of C0-SCC specimens after 2, 7 and 28 days of curing which are all reduced by increasing PC content especially at early age of curing. This fact may be due to various factors, such as using different superplasticizers or greater fines content in the SCCs. Roncero & Gettu (2002) have pointed out the formation of large CH crystals when using

Table 5. Compressive strength of C0-SCC specimens.

Sample designation	PC content (%)	Compressive strength (MPa)		
		2 days	7 days	28 days
C0-SCC0	0	16.9	25.4	34.8
C0-SCC0.3	0.3	15.7	24.3	34.0
C0-SCC0.5	0.5	15.1	23.2	33.1
C0-SCC0.7	0.7	14.5	22.0	32.5
C0-SCC1	1.0	14.0	20.6	31.6

polycarboxylate superplasticizers. These large crystals weaken the aggregate–paste transition zone and hence decrease the compressive strength of concrete by decreasing the aggregate–paste bond. As for the influence of the fines content, the bigger particles leads to the greater shrinkage (Song *et al* 2001 and Hammer *et al* 2001), giving rise to the appearance of a greater number of micro-cracks in the aggregate paste interface which also reduce the compressive strength. Moreover, by increasing the volume of fines, the specific surface area of the aggregates increases, with the aggregate–paste transition zone being precisely the weakest phase of the concrete.

During the early days of hydration, the strength is affected by two opposing effects: (i) the limestone fines raise the rate of hydration of some clinker compounds since the fines act as nucleation sites for the hydrates formed in the hydration reactions (Ye *et al* 2007). (ii) PC has a delaying effect on hydration of CH crystals and formation of C_3H (Puertas *et al* 2005a and 2005b).

At higher ages, 28 days, the two aforementioned effects disappear and it can clearly be seen that there is less effect on reducing the compressive strength in SCCs by increasing PC. This is due to a longer development over time for the cement's hydration processes in the SCCs with higher content of PC as a result of the SCCs' greater capacity to retain water (Puertas *et al* 2005a), which allows pozzolanic additions to continue reacting at higher ages with the lime resulting from the cement hydration. Furthermore, although PC retards the initial hydration reactions, according to Puertas *et al* (2005a) these reactions are intensified in later stages as a result of particle dispersion.

The pore structure of concrete is the general embodiment of porosity, pore size distribution, pore scale and pore geometry. The test results of MIP in this study include the pore structure parameters such as total specific pore volume, most probable pore diameter, pore size distribution, porosity, average diameter, and median diameter (volume). In terms of the different effect of pore size on concrete performance, the pore in concrete are classified as harmless (<20 nm),

Table 6. Total specific pore volumes and most probable pore diameters of C0-SCC specimens.

Sample designation	Total specific pore volume (mL/g)	Most probable pore diameter (nm)
C0-SCC0	0.0381	32
C0-SCC0.3	0.0346	24
C0-SCC0.5	0.0332	20
C0-SCC0.7	0.0320	18
C0-SCC1	0.0304	14

Table 7. Prosities, average diameters and median diameters (volume) of C0-SCC specimens.

Sample designation	Prosity (%)	Average diameter (nm)	Median diameter (volume) (nm)
C0-SCC0	8.99	27.53	41.4
C0-SCC0.3	8.11	20.9	30.3
C0-SCC0.5	7.70	16.8	28.7
C0-SCC0.7	7.46	12.1	25.4
C0-SCC1	7.17	10.2	22.2

low-harm (20–50 nm), harmful (50–200 nm) and very-harmful pore (>200 nm) (Wu & Lian 1999). In order to analyse and compare conveniently, the pore structure of concrete is divided into four ranges according to this sort method in this work.

Table 6 shows that with increasing PC content, the total specific pore volumes of concretes are decreased, and the most probable pore diameters shift to smaller pores and fall in the range of low-harm pore, which indicates that the addition of PC refines the pore structure of concretes.

Table 7 gives the porosities, average diameters and median diameters (volume) of various concretes. The regularity of porosity is similar to that of total specific pore volume. The regularity of average diameter and median diameter (volume) is similar to that of most probable pore diameter.

The pore size distribution of the concretes is shown in table 8. It is seen that by increasing PC content, the amount of pores decreases, which shows that the density is increased and the pore structure is improved.

Table 9 shows the results of conduction calorimetry of C0-SCC specimens. Two signals can be distinguished on all test results: a peak corresponding to the acceleration or post-induction period, associated with the precipitation of C–S–H gel and CH, and a shoulder related to a second, weaker signal with a later peak time, associated with the transformation from the ettringite (AFt) to the calcium monosulphoaluminate (AFm) phase via dissolution and reaction with $Al(OH)^{4-}$ (Jawed *et al* 1983). The numerical values corresponding to these two signals (heat release rate, peak times) and the total released heat are shown in table 9. The time period over the total heat was measured until the heat release rate was below 1% of the maximum of the second peak.

The heat release rate values in table 9 show that increasing the percentage of PC in the pastes retards peak times and raises heat release rate values. This is indicative of a delay in initial cement hydration because of higher content of PC. The retardation is much less marked in the second peak. The total heat released under identical conditions (at times when the heat release

Table 8. Pore size distribution of C0-SCC specimens.

Sample designation	Pore size distribution (mL/g(%))				Total specific pore volume (mL/g)
	Harmless pores (<20 nm)	Few-harm pores (20–50 nm)	Harmful pores (50–200 nm)	Multi-harm pores (>200 nm)	
C0-SCC0	0.0045	0.0127	0.0149	0.0079	0.0381
C0-SCC0.3	0.0044	0.0116	0.0121	0.0064	0.0346
C0-SCC0.5	0.0043	0.0108	0.0114	0.0056	0.0332
C0-SCC0.7	0.0041	0.0101	0.0108	0.0045	0.0320
C0-SCC1	0.0039	0.0090	0.0100	0.0038	0.0304

Table 9. Calorimetric results of C0–SCC specimens.

Sample designation	Total heat	First peak		Second peak	
	kJ/kg	Time (h)	Rate (W/kg)	Time (h)	Rate (W/kg)
C0-SCC0	319.8	1.8	0.62	16.1	2.71
C0-SCC0.3	333.5	1.9	0.64	17.2	2.86
C0-SCC0.5	345.3	2.1	0.67	18.6	3.02
C0-SCC0.7	359.5	2.25	0.69	19.5	3.29
C0-SCC1	371.7	2.4	0.71	20.6	3.41

Table 10. Weight loss (%) of the pastes in the range of 110–650°C at 28 days of curing of C0-SCC specimens.

Sample designation	Weight loss (%)
C0-SCC0	10.4
C0-SCC0.3	10.7
C0-SCC0.5	11.0
C0-SCC0.7	11.2
C0-SCC1	11.4

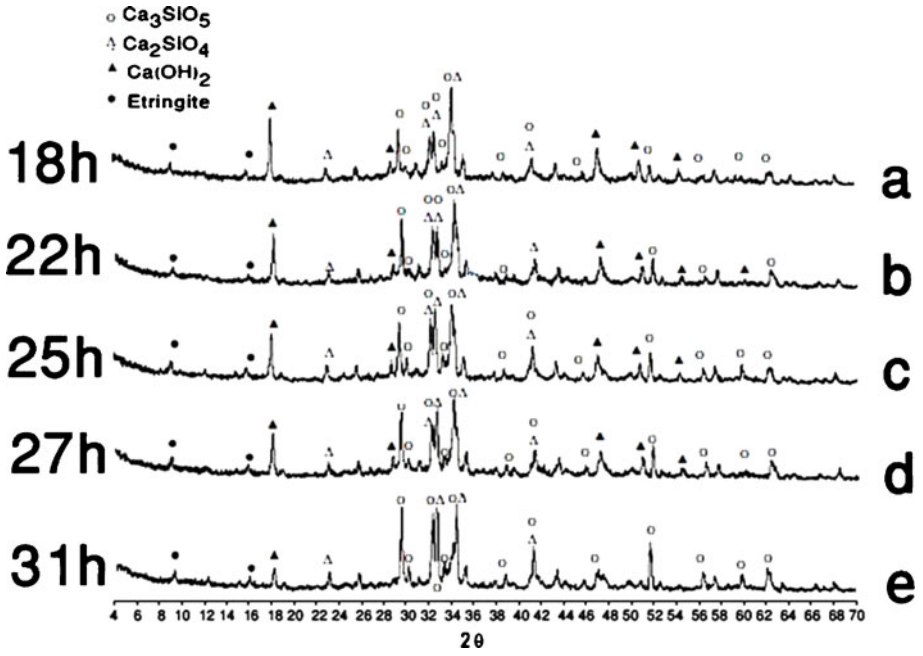

Figure 4. XRD results indicating the formation of hydrated products for different C0-SCC specimens: (**a**) C0-SCC0, (**b**) C0-SCC0.3, (**c**) C0-SCC0.5, (**d**) C0-SCC0.7 and (**e**) C0-SCC1.

rate is less than 1% of the maximum amount of heat released in the first peak) decreases with higher percentages of PC in the mix.

Table 10 shows the thermogravimetric analysis results of C0-SCC specimens measured in the 110–650°C range in which dehydration of the hydrated products occurred. The results show that after 28 days of curing, the loss in weight of the specimens is increased by decreasing the PC content in concretes.

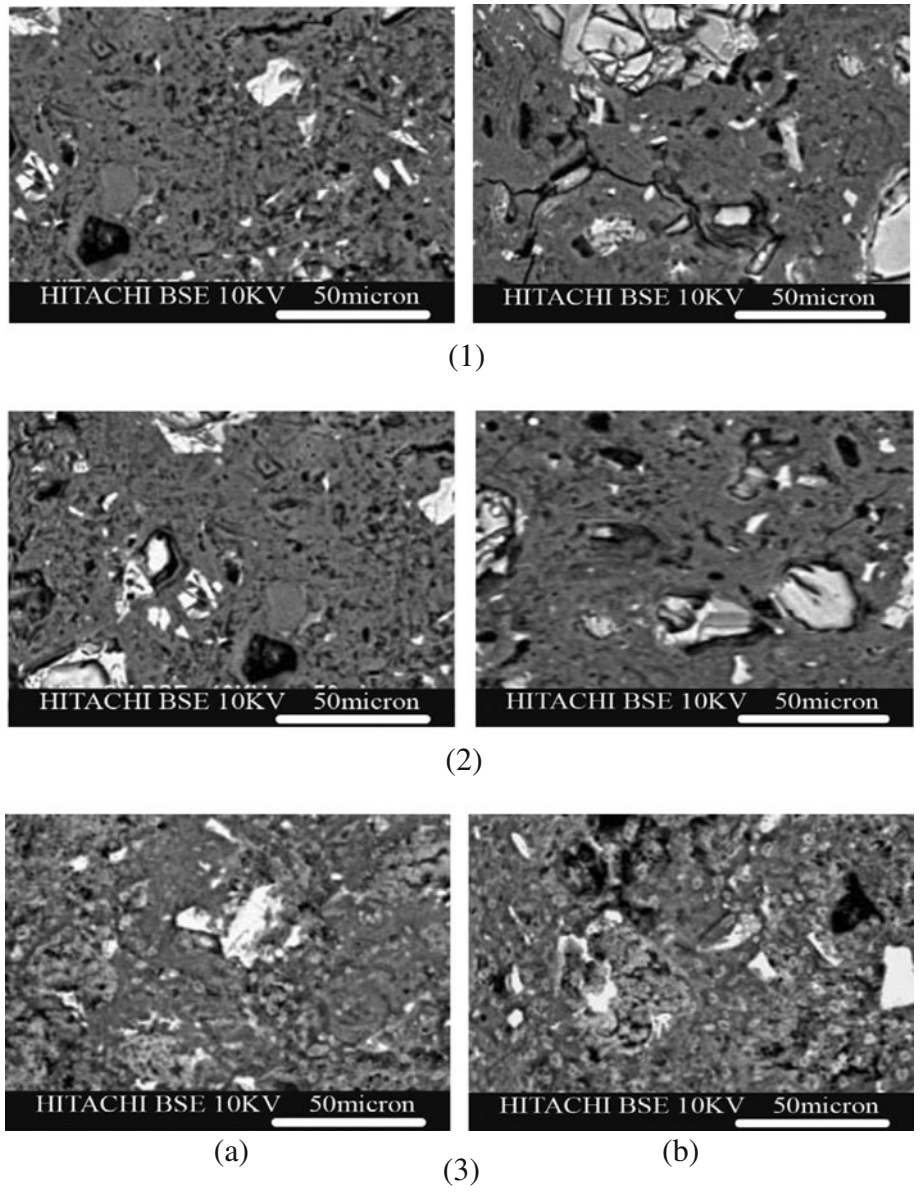

Figure 5. SEM micrographs of (**a**) C0-SCC0 specimen and (**b**) C0-SCC1 specimen at 2 days (series 1), 7 days (series 2) and 28 days (series 3) of curing.

Figure 4 shows XRD analysis of C0-SCC specimens at different times after curing. As figure 4 also shows, the peak related to formation of the hydrated products shifts to appear at later times indicating the negative impact of PC on formation of $Ca(OH)_2$ and C–S–H gel at early ages of cement hydration.

Finally, figure 5 shows SEM micrographs of C0-SCC specimens without and with PC. The morphological analysis evinced no substantial differences in either the form or the texture of the different reaction products in pastes with and without admixtures. The micrographs corresponding to paste cured for 2 and 7 days show anhydrous cement that has not yet reacted, along with a relatively porous mass analogous to the reaction products. This region is more compact and less porous in the paste with admixture. After 28 days, the reaction is observed to progress, with a considerable decrease in the amount of anhydrous cement particles.

The results obtained with respect to the effect of PC on cement hydration show that at early ages PC retards the initial cement hydration. This effect is more evident at higher doses of superplasticizer. This phenomenon is confirmed by the results obtained in conduction calorimetry, with a retardation of the peak time for the first peak in the heat release rate, associated with C_3H and CH formation. This lower initial formation of reaction products is further corroborated by the smaller weight loss detected in 2 day cured pastes with admixtures, when subjected to temperatures of 110–650°C. Such weight loss is related to the partial and total dehydration of C_3H and CH.

Since the amount of superplasticizer do not mainly affect on the compressive strength of the specimens while improve the workability of concrete, only cement paste with 1 wt.% PC admixture was selected because of its high workability and cement was partially replaced by different amount of CuO nanoparticles. The results are discussed in the following section.

3.2 *Strength analysis of N-SCC specimens*

Table 11 shows the compressive strength of N-SCC specimens after 2, 7 and 28 days of curing. The results show that the compressive strength increases by adding CuO nanoparticles up to 4.0wt.% replacement (N4-SCC series) and then it decreases, although adding 5.0 percent CuO nanoparticles produces specimens with much higher compressive strength with respect to the all other C0-SCC concretes. The reduced compressive strength by adding more than 4 wt.% CuO nanoparticles may be due to the fact that the quantity of CuO nanoparticles present in the mix is higher than the amount required to combine with the liberated lime during the process of hydration. This is leading to excess silica leaching out and causing a deficiency in strength as it replaces part of the cementitious material but does not contribute to strength. Also, it may be due to the defects generated in dispersion of nanoparticles that causes weak zones.

Table 11. Compressive strength of N-SCC specimens.

Sample designation	CuO nanoparticles (%)	Compressive strength (MPa)		
		2 days	7 days	28 days
N1-SCC1	1	13.9	22.5	32.9
N2-SCC1	2	15.1	27.0	35.8
N3-SCC1	3	16.6	30.4	41.6
N4-SCC1	4	17.7	35.2	46.9
N5-SCC1	5	19.0	33.1	45.6

Table 12. Total specific pore volumes and most probable pore diameters of N-SCC specimens.

Sample designation	Total specific pore volume (mL/g)	Most probable pore diameter (nm)
N1-SCC1	0.0268	11.2
N2-SCC1	0.0247	11.2
N3-SCC1	0.0229	10.3
N4-SCC1	0.0213	9.3
N5-SCC1	0.0223	10.3

The higher compressive strength in the N-SCC series mixtures with respect to C0-SCC series is due to the rapid consumption of crystalline $Ca(OH)_2$ which quickly forms during hydration of Portland cement, especially at early ages as a result of high reactivity of CuO nanoparticles. As a consequence, the hydration of cement is accelerated and larger volumes of reaction products are formed. Also, CuO nanoparticles recover the particle packing density of the blended cement, leading to a reduced volume of larger pores in the cement paste.

Table 12 shows that with increasing CuO nanoparticles up to 4 wt.%, the total specific pore volume of concrete decreases, and the most probable pore diameters reduces and falls in the range of low-harm pores, which indicates that the addition of PC refines the pore structure of concretes.

Table 13 gives the porosities, average diameters and median diameters (volume) of various concretes. The regularity of porosity is similar to that of total specific pore volume. The regularity of average diameter and median diameter (volume) is similar to that of most probable pore diameter.

The pore size distribution is shown in table 14. It is observed that by adding nanoparticles, the amount of pores is decreased, which shows that the density of concretes is increased and the pore structure is improved.

The effectiveness of nano-CuO in improving the pore structure of concretes increases in the order: N1-SCC <N2-SCC <N3-SCC <N5-SCC <N4-SCC. The mechanism by which the nanoparticles improve the pore structure of concrete can be interpreted as follows (Li *et al* 2007). Suppose that nanoparticles are uniformly dispersed in concrete and each particle is contained in a cube pattern, therefore the distance between nanoparticles can be determined. After the hydration begins, hydrate products diffuse and envelop nanoparticles as kernels (Li *et al* 2007). If the nanoparticle content and the distance between them are appropriate, the crystallization will be controlled through restricting the growth of $Ca(OH)_2$ crystals by nanoparticles. Moreover, the nanoparticles located in cement paste as kernels can further promote cement hydration due to their high activity. This makes the cement matrix more homogeneous and compact. Consequently, the pore structure of concrete is clearly improved such as the concrete containing nano-CuO in the amount of 1% by weight of binder (Li *et al* 2007).

Table 13. Prosities, average diameters and median diameters (volume) of N-SCC specimens.

Sample designation	Prosity (%)	Average diameter (nm)	Median diameter (volume) (nm)
N1-SCC1	6.51	9.3	19.9
N2-SCC1	6.22	8.9	18.5
N3-SCC1	6.02	8.3	15.4
N4-SCC1	5.82	7.7	11.4
N5-SCC1	5.91	8.0	13.6

Table 14. Pore size distribution of N-SCC specimens.

Sample designation	Pore size distribution (mL/g(%))				Total specific pore volume (mL/g)
	Harmless pores (<20 nm)	Few-harm pores (20–50 nm)	Harmful pores (50–200 nm)	Multi-harm pores (>200 nm)	
N1-SCC1	0.0035	0.0083	0.0089	0.0028	0.0267
N2-SCC1	0.0033	0.0078	0.0083	0.0024	0.0247
N3-SCC1	0.0030	0.0070	0.0066	0.0018	0.0229
N4-SCC1	0.0027	0.0063	0.0047	0.0013	0.0213
N5-SCC1	0.0028	0.0066	0.0060	0.0016	0.0223

With increasing the CuO nanoparticle content above 4 wt.%, the improvement in the pore structure is weakened. This can be attributed to the distance between nanoparticles decreasing with increasing nanoparticle content, and $Ca(OH)_2$ crystals cannot grow enough due to limited space and the crystal quantity is decreased, which leads to the ratio of crystal to strengthening gel being low and the shrinkage and creep of the cement matrix increased (Ye 2001), thus the pore structure of the cement matrix is loosened relatively.

On the whole, the addition of nanoparticles improves the pore structure of concrete. On one hand, nanoparticles can act as a filler to enhance the density of concrete, which leads to the porosity of concrete being reduced significantly. On the other hand, nanoparticles can not only act as an activator to accelerate cement hydration due to their high activity, but also act as a kernel in cement paste which reduces the size of $Ca(OH)_2$ crystal and the tropism more stochastic.

The heat release rate values in table 15 show that increasing the percentage of CuO nanoparticles up to 4 wt.% in the pastes accelerates peak times and drops heat release rate values. This is indicative of acceleration in initial cement hydration due to higher content of CuO nanoparticles. CuO nanoparticles as a nucleation site can accelerate the cement hydration and hence increase the heat release rate. As stated above, the appearance of the peaks in conduction calorimetry tests are due to CH and C_3H compound formation in the cement paste. When CuO nanoparticles are added to cement paste, the acceleration in formation of CH and C_3H would result in more rapid appearance of the related peaks.

Table 16 shows the thermogravimetric analysis results of N-SCC specimens measured in the 110–650°C range in which dehydration of the hydrated products occurred. The results show that after 28 days of curing, the loss in weight of the specimens is increased by increasing CuO nanoparticles in concretes up to 4wt.%. Again, as with the results obtained for conduction

Table 15. Calorimetric results of N-SCC specimens.

Sample designation	Weight loss	First peak		Second peak	
	(%)	Time (h)	Rate (W/kg)	Time (h)	Rate (W/kg)
N1-SCC1	304.0	2.0	0.60	16.3	2.66
N2-SCC1	277.8	1.7	0.57	15.2	2.35
N3-SCC1	263.4	1.4	0.54	13.6	2.08
N4-SCC1	243.4	1.1	0.49	12.0	1.88
N5-SCC1	257.3	1.3	0.51	12.9	2.01

Table 16. Weight loss (%) of the pastes in the range of 110–650°C at 28 days of curing of N-SCC specimens.

Sample designation	Weight loss (%)
N1-SCC1	10.4
N2-SCC1	10.3
N3-SCC1	10.1
N4-SCC1	10.0
N5-SCC1	9.8

calorimetry, the increase in weight loss is due to more formation of CH and C_3H compounds in the cement paste.

Figure 6 shows XRD analysis of N-SCC specimens at different times after curing. As figure 6 also shows, the peak related to formation of the hydrated products shifts to appear in earlier times indicating the positive impact of PC on formation of $Ca(OH)_2$ and C–S–H gel at early age of cement hydration.

Finally, figure 7 shows SEM micrographs of N-SCC specimens containing 4 wt.% of CuO nanoparticles. Figure 7 shows a more compact mixture after all days of curing which indicate rapid formation of C–S–H gel in presence of CuO nanoparticles.

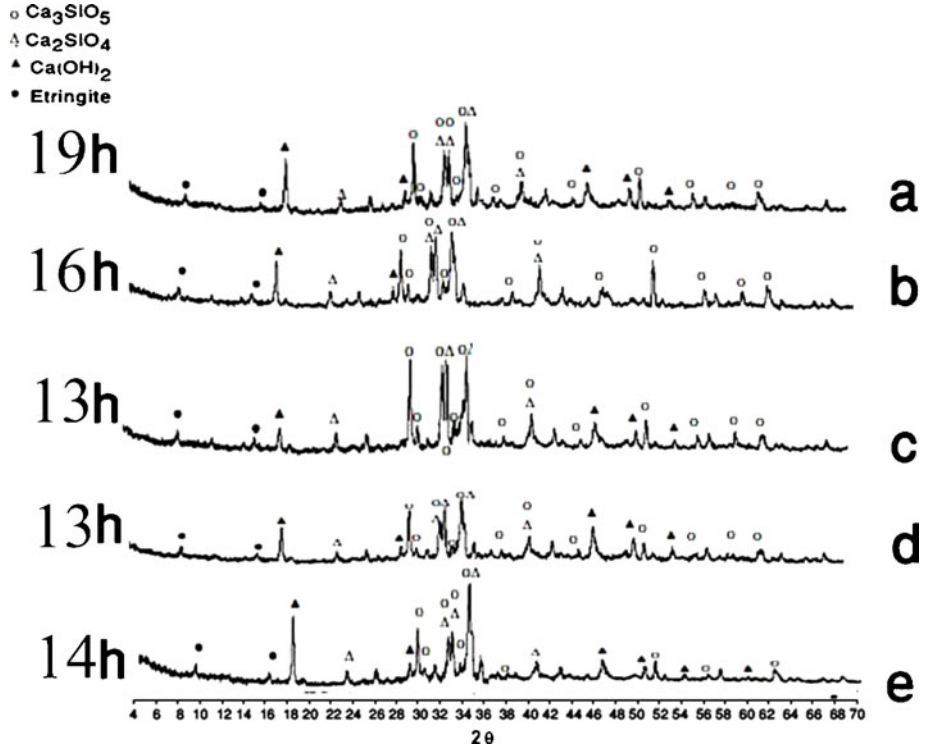

Figure 6. XRD results indicating the formation of hydrated products for different N-SCC specimens: (**a**) N1-SCC1, (**b**) N2-SCC1, (**c**) N3-SCC1, (**d**) N4-SCC1 and (**e**) N5-SCC1.

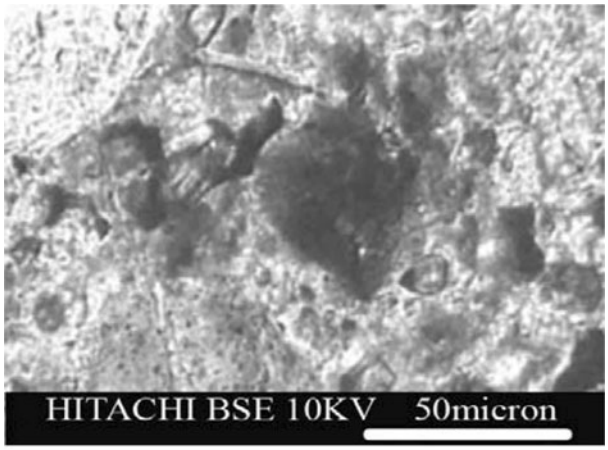

(1)

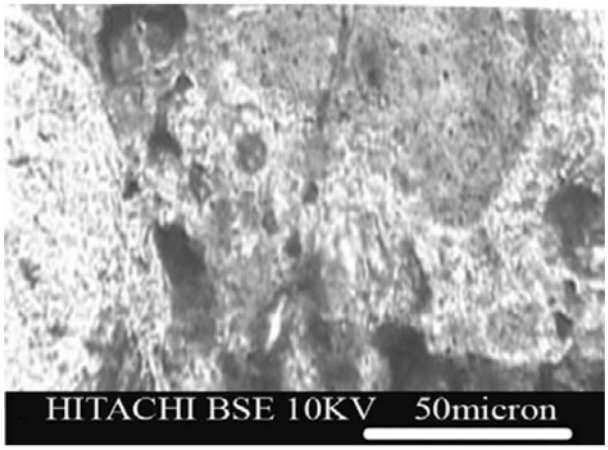

(2)

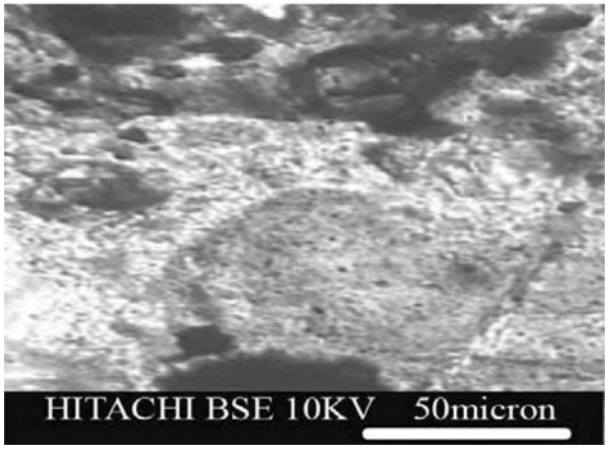

(3)

Figure 7. SEM micrographs of N4-SCC1 specimen at 2 days (1), 7 days (2) and 28 days (3) of curing.

Some studies have been conducted on compressive strength of cementitious composites reinforced by nano-particles and some possible reasons have been represented to show the increment of compressive strength.

(i) When a small amount of the nano-particles is uniformly dispersed in the cement paste, the nano-particles act as a nucleus to tightly bond with cement hydrate and further promote cement hydration due to their high activity, which is favourable for the strength of cement mortar (Flores-Velez & Dominguez 2002).
(ii) The nano-particles among the hydrate products will prevent crystals from growing which are positive for the strength of cement paste (Grzeszczyk & Lipowski 1997; Fernandez *et al* 1999 and Flores-Velez & Dominguez 2004).
(iii) The nano-particles fill the cement pores, thus increasing the strength. Nano–CuO can contribute in the hydration process to generate C–S–H through reaction with $Ca(OH)_2$ (Massazza 1987).

In this paper, the strength enhancement under compressive force has been investigated energetically:

Both nanoparticles and aggregates are exterior particles but the reason why the nanoparticles are able to make a stronger composite is as a result of the free energy of nucleation sites. The driving force for the nucleation is the reduction in interfacial free energy between the nucleus (C–S–H gel) and nucleation site (nanoparticle or aggregates). In comparison between these two approximately spherical particles (nanoparticle and aggregates), the ratio between surface area to volume of nanoparticle is much larger than that of aggregates. Therefore, the interaction between the nanoparticles with CH crystals and formation of C–S–H gel is more accessible than this reaction between the aggregates and CH crystals.

In addition, the C–S–H gel-nanoparticle interface is probably coherent or semi-coherent. This is due to this fact that C–S–H gel formed around the nanoparticle could maintain its coherency with the nanoparticle because both C–S–H gel and nanoparticle have nano-scale dimensions. But the C–S–H gel formed around the aggregate has a completely incoherent interface with aggregate. In other words, the sand particle is too large to maintain its coherency with nanoscale C–S–H gel. Furthermore, in the vicinity of the aggregates, the probability of void formation and presence of un-reacted cement, other aggregates and even nanoparticles is much more with respect to the nanoparticle and causes more weak zones in the vicinity of sand. Although sands act as reinforcement in cementitious matrix, as a result of incoherency under compressive loading, fracture occurrence and crack propagation from the C–S–H gel formed at the surface of the sand is more probable with respect to the nanoparticle. This phenomenon is very similar to the effects inclusions and precipitations in metallic alloys where inclusions with incoherent interface (like aggregate in concrete) can not improve the mechanical properties of the alloy while precipitates with coherent or semi-coherent interfaces (like nanoparticles in concrete) can improve mechanical properties of the alloy. Therefore, the smaller nanoparticle size leads to the generation of heterogeneous nucleation sites and hence shorter early age according to Eq. (2) (Porter & Easterling 1992; Müller 2007);

$$I = A.N_T.\exp\left(\frac{-\Delta G^*}{kT}\right), \tag{2}$$

where I the nucleation rate,
ΔG^* the critical free energy for nucleation,
T the absolute temperature,

k the Bultzman's constant,
A a constant and
N_T the number of nucleation sites.

In a constant temperature, by increasing N_T (the smaller nanoparticles) the rate of C–S–H gel formation is increased causes shorter early age.

In general, the free energy of heterogeneous nucleation from gel on the surface of a foreign particle (ΔG_{het} which here is CuO in the form of aggregate or nanoparticle) could be obtained from Eq. (3) (Lu & Young 1992; Lin *et al* 2004);

$$\Delta G_{het} = -V_S.\Delta G_V + A_{sg}.\gamma_{sg} + A_{sp}.\gamma_{sp} - A_{sp}.\gamma_{pg}, \tag{3}$$

where V_S the volume of solid nucleus,
ΔG_V the volume energy of solid nucleus,
A_{sg} the interface between solid nucleus and gel,
A_{sp} the interface between solid nucleus and nanoparticle,
γ_{sg} the surface free energy between solid nucleus and gel,
γ_{sp} the interface between solid nucleus and nanoparticle and
γ_{pg} the surface free energy between nanoparticle and gel.

The negative signs are due to conversion of gel to solid nucleus. In heterogeneous nucleation, to minimize ΔG^*, the nucleus shape must be a part of hemisphere (figure 8). The values of V_S, A_{sg} and A_{sp} could be obtained as (Lu & Young 1992; Porter & Easterling 1992):

$$V_S = \frac{\pi r^3 (2 + \cos\theta)(1 - \cos\theta)^2}{2\pi r^2 (1 - \cos\theta)} \tag{4}$$

$$A_{sg} = 2\pi r^2 (1 - \cos\theta) \tag{5}$$

$$A_{sp} = \pi r^2 \sin^2\theta, \tag{6}$$

where r the nucleus radius and θ the wetting angle and is constant during the growth of nucleus (figure 8).

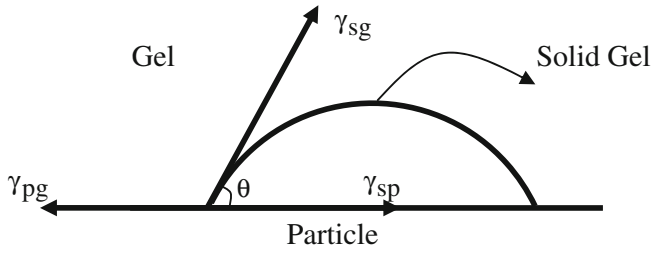

Figure 8. Heterogeneous nucleation of C–S–H gel upon the sands and nanoparticles.

Figure 8 shows that the equilibrium condition is obtained when (Porter & Easterling 1992):

$$\gamma_{pg} = \gamma_{sp} + \gamma_{pg}\cos\theta \text{ or } \cos\theta = \frac{\gamma_{pg} - \gamma_{sp}}{\gamma_{sg}}. \tag{7}$$

By substituting of Eqs. (4)–(7) into Eq. (3) one may write (Porter & Easterling 1992):

$$\Delta G_{het} = \left(-\frac{4}{3}\pi r^3 \Delta G_V + 4\pi r^2 \gamma_{sg}\right).S(\theta), \tag{8}$$

where S(θ) is the shape factor and could be written as (Porter & Easterling 1992):

$$S(\theta) = \frac{(2+\cos\theta)(1-\cos\theta)^3}{4}. \tag{9}$$

The critical radius of nucleation (r*) could be obtained from the first derivative of Eq. (8) with respect to r and equalling to zero (Porter & Easterling 1992; Baierlein 2003):

$$r^* = \frac{2\gamma_{sg}}{\Delta G_V}. \tag{10}$$

By substituting Eq. (10) into Eq. (8) one may write (Porter & Easterling 1992):

$$\Delta G^* = \frac{16\pi\gamma_{sg}^3}{3\Delta G_V^2}.S(\theta), \tag{11}$$

γ_{sg} and ΔG_V depend on the particle composition and are equal for different particle sizes. Eq. (11) shows that by decreasing θ, ΔG^* is also decreased. If both nucleus and nucleation site have the same crystalline structure and have approximately equal cell parameters, then γ_{sp} could be maintained at its minimum amount and according to Eq. (7), θ is minimized.

From this point of view, ΔG^* could be different for nanoparticles and aggregates and may be greater for aggregates. On the other hand, Eq. (11) could be written as (Porter & Easterling 1992);

$$\begin{aligned}\Delta G^* &= \frac{2}{3}\pi\left(\frac{2\gamma_{sg}}{\Delta G_V}\right)^3.\Delta G_V.\frac{(2+\cos\theta)(1-\cos\theta)^3}{4} \\ &= \frac{\pi (r^*)^3 (2+\cos\theta)(1-\cos\theta)^3}{4}.\frac{1}{2}\Delta G_V = \frac{1}{2}V^*\Delta G_V,\end{aligned} \tag{12}$$

where V* is the critical volume of nucleus.

The difference between nucleation on aggregates and nanoparticles is in the volume of nucleated material for reaching to r*. C–S–H gel which is formed around the sand propagates over the time and makes a large amount of C–S–H gel with incoherent interface since its critical volume probably reaches to r*.

4. Conclusions

The results obtained in this study can be summarized as follows.

(i) The increased PC content results in decreased compressive strength. It has been argued that PC retards cement hydration especially at early ages. However, there were no evident differences between compressive strength of specimens with and without PC.

(ii) As the CuO nanoparticle content is increased up to 4 wt.%, the compressive strength of SCC specimens is increased. This is due to more formation of hydrated products in the presence of CuO nanoparticles.
(iii) CuO nanoparticles up to 4 wt.% could accelerate the appearance of the first peak in conduction calorimetry testing which is related to the acceleration in formation of hydrated cement products.
(iv) Thermogravimetric analysis shows that CuO nanoparticles could increase the weight loss of the specimens when partially added to cement paste up to 4 wt.%. More rapid formation of hydrated products in the presence of CuO nanoparticles (which was confirmed by XRD results) could be the reason for more weight loss.
(v) The pore structure of self compacting concrete containing CuO nanoparticles is improved and the content of all mesopores and macropores is decreased.

References

Abell A B, Willis K L and Lange D A 1999 Mercury Intrusion Porosimetry and Image nalysis of Cement-Based Materials, *J. Colloid Interface Sci.* 211: 39–44

Baierlein R 2003 Thermal physics. Cambridge University Press. ISBN 0-521-658381

Bjornstrom J, Martinelli A, Matic A, Borjesson L and Panas I 2004 Accelerating effects of colloidal nano-silica for beneficial calcium–silicate–hydrate formation in cement, *Chem. Phys. Lett.* 392(1–3): 242–248

Bosiljkov V B 2003 SCC mixes with poorly graded aggregate and high volume of limestone filler, *Cem. Concr. Res.* 33(9): 1279–1286

Campillo I, Guerrero A, Dolado J S, Porro A, Ibáñez J A and Goñi S 2007 Improvement of initial mechanical strength by nanoalumina in belite cements, *Mater. Lett.* 61: 1889–1892

Chopin D, Francy O, Lebourgeois S and Rougeau P 2003 'Aleep and shrinkage of heat-cured self compacting concrete (SCC)', In: O Wallevik and I Nielsson, (eds.), *Proceedings of the 3rd international RILEM symposium on self-compacting concrete*, RILEM Publications S.A.R.L., Reykjavik, 672–683

Daoud A, Lorrain M and Laborderie C 2003 'Anchorage and cracking behaviour of self-compacting concrete', In: O Wallevik and I Nielsson, (eds.) *Proceedings of the 3rd international RILEM symposium on self compacting concrete*, RILEM Publications S.A.R.L., Reykjavik, 692–702

Fava C, Bergol L, Fornasier G, Giangrasso F and Rocco C 2003 'Fracture behaviour of self–compacting concrete', In: O Wallevik and I Nielsson, (eds.) *Proceedings of the 3rd international RILEM symposium on self-compacting concrete*, RILEM Publications S.A.R.L., Reykjavik, 628–636

Fernandez E, Gil F J, Ginebra M P, Driessens F C M, Planell J A and Best S M 1999 'Production and characterisation of new calcium phosphate bone cements in the CaHPO4-a-Ca3(PO4)2 system: pH, workability and setting times', *J. Mater. Sci. Mater. Med.* 10: 223–230

Flores-Velez L M and Dominguez O 2002 'Characterization and properties of Portland cement composites incorporating zinc-iron oxide nanoparticles', *J. Mater. Sci.* 37: 983–988

Grzeszczyk S and Lipowski G 1997 'Effect of content and particle size distribution of high calcium fly ash on the rheological properties of cement pastes', *Cem. Concr. Res.* 27(6): 907–916

Hammer T A, Johansen K and Bjøntegaard Ø 2001 'Volume changes as driving forces to self-induced cracking of norwegian SCC', In: K Ozawa and M Ouchi, (eds.) *Proceedings of the 2nd international RILEM symposium on self-compacting concrete*, Published by COMS Engineering Corporation, Tokyo, 423–432

Hauke B 2001 'Self-compacting concrete for precast concrete products in Germany', In: K Ozawa and M Ouchi, (eds.) *Proceedings of the 2nd international RILEM symposium on self-compacting concrete*, Published by COMS Engineering Corporation, Tokyo, 633–642

Jawed J, Skalny J and Young J F 1983 '*Hydration of Portland Cement. Structure and Performance of Cements*, P Barnes (ed.)', Essex: Applied Science Publishers, 284–285

Ji T 2005 'Preliminary study on the water permeability and microstructure of concrete incorporating nano-SiO2', *Cem. Concr. Res.* 35(10): 1943–1947

Jo B-W, Kim C-H, Tae G-h and Park J-B 2007 'Characteristics of cement mortar with nano-SiO2 particles', *Construct. Build. Mater.* 21(6): 1351–1355

Klug Y and Holschemacher K 2003 'Comparison of the hardened properties of self-compacting and normal vibrated concrete', In: O Wallevik and I Nielsson, (eds.) *Proceedings of the 3rd international RILEM symposium on self-compacting concrete*, RILEM Publications S.A.R.L., Reykjavik, 596–605

Köning G, Holsechemacher K, Dehn F and Weiβe D 2001 'Self-compacting concrete-time development of material properties and bond behavior', In: K Ozawa and M Ouchi, (eds.) *Proceedings of the 2nd international RILEM symposium on self-compacting concrete*, Published by COMS Engineering Corporation, Tokyo, 507–516

Li H, Xiao H and Ou J 2004 'A study on mechanical and pressure-sensitive properties of cement mortar with nanophase materials', *Cement and Concrete Res.* 34: 435–438

Li H, Zhang M and Ou J 2007 'Flexural fatigue performance of concrete containing nanoparticles for pavement', *Int. J. Fatigue*, 29: 1292–1301

Li Z, Wang H, He S, Lu Y and Wang M 2006 'Investigations on the preparation and mechanical properties of the nano-alumina reinforced cement composite', *Mater. Lett.* 60: 356–359

Lin Y H, Tyan Y Y, Chang T P, Chang C Y 2004 An assessment of optimal mixture for concrete made with recycled concrete aggregates. *Cem. Concr. Res.* 34(8): 1373–1380

Lu P, Young J F 1992 Hot pressed DSP cement paste, *Material Res. Soc. Symposium Proceedings*, 245

Makishima O, Tanaka H, Itoh Y, Komada K and Satoh F 2001 'Evaluation of mechanical properties and durability of super quality concrete', In: K Ozawa and M Ouchi, (eds.) *Proceedings of the 2nd international RILEM symposium on self-compacting concrete*, Published by COMS Engineering Corporation, Tokyo, 475–482

Massazza F 1987 'The role of the additions to cement in the concrete durability', *Cemento* 84: 359–382

Müller I 2007 A history of thermodynamics - The doctrine of energy and entropy. Springer. ISBN 978-3-540-46226-2

Nazari A 2010 The effects of curing medium on flexural strength and water permeability of concrete incorporating TiO_2 nanoparticles, *Mater. Struct.* doi:10.1617/s11527-010-9664-y

Nazari A, Riahi S 2010a Microstructural, thermal, physical and mechanical behavior of the self compacting concrete containing SiO2 nanoparticles, *Mater. Sci. Eng. A* 527: 7663–7672

Nazari A, Riahi S 2010b The effects of TiO_2 nanoparticles on flexural damage of self-compacting concrete, *Int. J. Damage Mech.* doi:10.1177/1056789510385262

Nazari A, Riahi S 2010c The effect of TiO_2 nanoparticles on water permeability and thermal and mechanical properties of high strength self-compacting concrete, *Mater. Sci. Eng. A*. doi:10.1016/j.msea.2010.09.074

Nazari A, Riahi S 2010d The effects of zinc dioxide nanoparticles on flexural strength of self-compacting concrete, Composites Part B: Engineering, doi:10.1016/j.compositesb.2010.09.001

Nazari A, Riahi S 2010e The effects of ZnO_2 nanoparticles on split tensile strength of self-compacting concrete, *J. Exp. Nanoscience.* doi:10.1080/17458080.2010.524669

Nazari A, Riahi S 2010f Limewater effects on properties of ZrO_2 nanoparticle blended cementitious composite, *J. Compos. Mater.* doi:10.1177/0021998310376118

Nazari A, Riahi S 2010g Assessment of the effects of Fe_2O_3 nanoparticles on water permeability, workability, and setting time of concrete, *J. Compos. Mater.* doi:10.1177/0021998310377945

Nazari A, Riahi S 2010h The effects of limewater on flexural strength and water permeability of Al_2O_3 nanoparticles binary blended concrete, *J. Compos. Mater.* doi:10.1177/0021998310378907

Nazari A, Riahi S 2010i The effects of limewater on split tensile strength and workability of Al_2O_3 nanoparticles binary blended concrete, *J. Compos. Mater.* doi:10.1177/0021998310378909

Nazari A, Riahi S 2010j The effects of TiO_2 nanoparticles on properties of binary blended concrete, *J. Compos. Mater.* doi:10.1177/0021998310378910

Nazari A, Riahi S 2010k Optimization mechanical properties of Cr_2O_3 nanoparticle binary blended cementitious composite, *J. Compos. Mater.* doi:10.1177/0021998310377944

Porter D A and Easterling K E 1992 *Phase Transformation in Metals and Alloys*, 2nd ed. London: Chapman Hall

Puertas F, Santos H, Palacios M and Martínez-Ramírez S 2005a 'Polycarboxylate superplasticiser admixtures: effect on hydration, microstructure and rheological behavior', *Advances in Cement Res.* 17(2): 77–89

Puertas F, Alonso M M and Vázquez T 2005b 'Effect of polycarboxylate admixtures on portland cement paste setting and rheological behavior', *Materiales de Construcción* 55(277): 61–73

Roncero J and Gettu R 2002 'Influencia de los superplastificantes en la microestructura de la pasta hidratada y en el comportamiento diferido de los morteros de cement', *Cemento Hormigón* 832: 12–28

Song H W, Byun K J, Kim S H and Choi D H 2001 'Early-age creep and shrinkage in self-compacting concrete incorporating GGBFS', In: K Ozawa and M Ouchi, (eds.) *Proceedings of the 2nd international RILEM symposium on self-compacting concrete*, Published by COMS Engineering Corporation, Tokyo, 413–422

Su N, Hsu K and Chai H 2001 'A simple mix design method for self-compacting concrete', *Cement and Concrete Res.* 31(12): 1799–1807

Tanaka K and Kurumisawa K 2002 'Development of technique for observing pores in hardened cement paste', *Cement and Concrete Res.* 32: 1435–1441

Wu Z W and Lian H Z 1999 '*High performance concrete*', Beijing: Railway Press of China, 43

Ye Q 2001 'The study and development of the nano-composite cement structure materials', *New Building Materials*, 1: 4–6

Ye G, Xiu X, De Schutter G, Poppe A M, Taerwe L 2007 Influence of limestone powder as filler in SCC on hydration and microstructure of cement pastes, *Cem. Concr. Compos.* 29(2): 94–102

Zivica V 2009 'Effects of the very low water/cement ratio', *Constr. Build. Mater.* 23(8): 2846–2850